Invited Paper

Material and process optimization for EUV pattern rectification by DSA

Lander Verstraete*[a], Hyo Seon Suh[a], Julie Van Bel[a], Byeong-U Bak[a,b], Seong Eun Kim[a,c], Remi Vallat[a], Philippe Bezard[a], Matteo Beggiato[a], Christophe Beral[a]

[a]Imec, Kapeldreef 75, 3001 Leuven, Belgium
[b]Department of Photonics and Nanoelectronics, Hanyang University, Ansan 15588, Republic of Korea
[c]School of Chemical and Biological Engineering, Institute of Chemical Processes, Seoul National University Seoul 08826, Republic of Korea

*Corresponding email: Lander.Verstraete@imec.be

ABSTRACT

Continuous scaling by extreme ultraviolet (EUV) lithography is tightening the patterning requirements for photoresist materials. Specifically, chemically amplified resists (CAR) are facing significant challenges to keep supporting the patterning needs. In view of this, complementing EUV lithography with directed self-assembly (DSA) of block copolymers offers interesting opportunities to enable the use of CAR towards ultimate resolution. As DSA decouples the resist patterning performance from the final pattern quality, roughness and defects in the resist pattern can be rectified. Here, we discuss the impact of material and process parameters on the rectification performance by DSA, both for line-space and hexagonal contact hole arrays.

Keywords: Directed Self-Assembly, EUV Lithography, Pattern Rectification, PS-b-PMMA, EUV stochastics

1. INTRODUCTION

To ensure continuous scaling of device features for the next generation technology nodes, EUV lithography is now being adopted by the semiconductor industry. Simultaneously, this continuous decrease of pattern dimensions is tightening the patterning requirements for photoresist materials. EUV resists should combine high resolution with low roughness, high sensitivity, and sufficient etch budget for pattern transfer. This is greatly challenging existing polymeric resist platforms based on chemical amplification (CAR). While CAR materials have made significant progress since their first invention,[1] meeting all the specifications for printing tight pitch EUV patterns is not trivial. Firstly, CAR is prone to stochastic variations in the printed pattern. This can be attributed to inhomogeneous distribution of components such as photo-acid generator and quencher, but also to the polydispersity and finite size of the polymer backbones.[2] Secondly, non-metal containing resists such as CAR have relatively low EUV absorption cross section necessitating high EUV doses.[3,4] Finally, as resist thickness also needs to scale down in order to avoid pattern collapse, the available process window for pattern transfer etch with CAR is narrowing down.

To alleviate the tight photoresist requirements, directed self-assembly (DSA) has proven to be an effective technology to rectify EUV resist patterns.[5-9] Here, block copolymers (BCP) are used to reconstruct a line-space (L/S) or hexagonal contact hole (HEXCH) resist pattern from the bottom-up. To do so, the resist pattern is converted into a guide pattern on top of which a BCP film can undergo phase separation to induce the corresponding L/S or HEXCH structure. As the final pattern is determined by phase separation of the BCP, DSA is relatively tolerant to small variations in the guide pattern. This allows to decouple the resist patterning performance from that of the final DSA pattern. As such, DSA can heal stochastic defects, and improve roughness or local CD uniformity (LCDU). This might enable the use of CAR materials for defining pattern features at ultimate resolution. Moreover, this could be achieved at attractive EUV dose.

In this work, the possibility for reducing EUV dose by 60% using DSA is demonstrated for L/S patterns. Next, the impact of BCP material and guide pattern contrast on bridge defect formation for pitch 28 nm and 24 nm L/S patterns is discussed.

Novel Patterning Technologies 2024, edited by J. Alexander Liddle, Ricardo Ruiz,
Proc. of SPIE Vol. 12956, 129560G · © 2024 SPIE
0277-786X · doi: 10.1117/12.3010817

In addition, rectification of pitch$_{C2C}$ 32 nm and 30 nm is described with a focus on how to improve LCDU and local pattern placement error (LPPE) by BCP material optimization. In case pitch$_{C2C}$ 32 nm HEXCH patterns, a detailed e-beam inspection is conducted showcasing how minimum defectivity for DSA contact hole patterns can be achieved.

2. METHODOLOGY

2.1 Rectification process flow

The rectification process flow used in this work is illustrated in previous work.[8] Unless stated otherwise, the process flow starts by coating a thin cross-linked polystyrene (X-PS) underlayer on a 13 nm SiN layer deposited on a 300 mm Si wafer. CAR resist is subsequently patterned using an NXE:3400B scanner from ASML. Using an oxidizing surface treatment, the resist pattern is transferred into the underlayer and the remaining photoresist is stripped with Microstrip®6800 on a dedicated cleaning tool. A poly(styrene-*block*-methyl methacrylate) (PS-*b*-PMMA) block copolymer (BCP) is then spincoated on the guide pattern and annealed under a low oxygen environment on a DT-3000 track from SCREEN. The BCP patterns are finally etched into the SiN layer using dry etch. In case of HEXCH patterns, the PMMA is first removed by a wet development process on the DT-3000 track.

2.2 Surface free energy measurements

Contact angles for different underlayers were measured with water and diiodomethane using a Dataphysics OCAH230L contact angle tool. Contact angle values were taken as the average from three measurement points. Using the contact angle data, surface free energy values of the underlayers were estimated using the harmonic mean equation as shown in Eq. 1:

$$0.25\gamma_l(1+cos\theta_Y) = \left[\frac{\gamma_{UL}^d\gamma_l^d}{(\gamma_{UL}^d+\gamma_l^d)} + \frac{\gamma_{UL}^p\gamma_l^p}{(\gamma_{UL}^p+\gamma_l^p)}\right], \quad (1)$$

where γ_{UL} is the surface free energy of the underlayer, γ_l is the surface tension of the probing liquid and θ_Y is the contact angle. γ^d and γ^p refer to the dispersive and polar components of the surface free energies, respectively. The surface energies for the pristine underlayers were obtained after coating EUV resist, applying the surface treatment, and stripping the photoresist with Microstrip®6800. The surface energies for the treated underlayers were obtained after coating EUV resist, EUV exposure (including PEB and development), applying the surface treatment, and stripping with Microstrip®6800.

To estimate the wetting behavior of different underlayers *versus* a polystyrene (PS) or polymethylmethacrylate (PMMA) block, the interfacial energies were calculated using the harmonic mean equation shown in Eq. 2.

$$\gamma_{UL-PS/PMMA} = \gamma_{UL} + \gamma_{PS/PMMA} - 4\left[\frac{\gamma_{UL}^d\gamma_{PS/PMMA}^d}{(\gamma_{UL}^d+\gamma_{PS/PMMA}^d)} + \frac{\gamma_{UL}^p\gamma_{PS/PMMA}^p}{(\gamma_{UL}^p+\gamma_{PS/PMMA}^p)}\right], \quad (2)$$

where $\gamma_{UL-PS/PMMA}$ is the interfacial energy of the underlayer with PS or PMMA, and $\gamma_{PS/PMMA}$ is the surface free energy of PS or PMMA. The latter values were taken from the literature.[10] Finally, the wetting behavior was quantified by $\Delta\gamma$ according to Eq. 3

$$\Delta\gamma = \gamma_{UL-PS} - \gamma_{UL-PMMA}. \quad (3)$$

2.3 Characterization and metrology

Patterns on the wafer were examined using a Hitachi CG-6300 critical dimension scanning electron microscopy (CDSEM) tool. For extraction of roughness, the following imaging conditions were chosen: *magnification* = 82.400; *pixels* = 2048×2048; *number of frames* = 32; *number of images* ≥ 50. For analysis of bridge defects from CDSEM images, imaging conditions were chosen as follows: *magnification* = 82.400; *pixels* = 2048×2048; *number of frames* = 32; *number of images* = 30. For measurement of LCDU and LPPE the following imaging conditions were used: *magnification* = 82.400; *pixels* = 2048×2048; *number of frames* = 16 (after wet development) or 32 (after SiN etch); *number of images* = 20; *scan type* = Mobius (non-unique). All metrology was performed by offline image analysis using MetroLER™ version 4.1.0.0 (Fractilia, LCC). In case of LPPE, the average of X LPPE and Y LPPE is taken and reported.

BCP pitch (L_0) for HEXCH patterning was measured by coating the BCP material on a neutral brush layer and baking under a low oxygen environment. The PMMA block was removed using a wet development step prior to CDSEM inspection. The following imaging conditions were used: *magnification* = 100.000; *pixels* = 2048×2048; *number of frames*

= 16; *number of images* = 20. The L_0 values were extracted using DSA-APPS (Hitachi High-Tech), and the average number from 20 images is reported.

Optical defect inspection of pitch 28 nm L/S patterns etched into 13 nm SiN was performed on a KLA-Tencor 2935 inspection tool operating in dark field mode. Subsequent defect review was performed using a KLA-Tencor ebeam review (EDR7380) tool, and defects were classified manually. Defectivity analysis of HEXCH patterns after etch into a 13 nm SiN layer was performed by acquiring a large number of SEM images on an Provision2E tool from Applied Materials. Imaging conditions used to acquire the images are: *field of view* = 2 µm×2 µm; *pixels* = 1000×1000; *number of frames* = 16. Detection and classification of defects for HEXCH patterns was performed using an in-house developed machine learning algorithm (YOLOv8).[11]

3. RESULTS AND DISCUSSION

2.1 L/S pattern rectification

A consequence of the pattern rectification ability by DSA, is the prospect of working at attractive EUV dose. To demonstrate this, three different CAR resists were selected with different EUV sensitivity for printing pitch 28 nm L/S patterns. As evident from Figure 1, the uLWR value of the resist patterns increases as EUV dose is being reduced. This observation illustrates the R(esolution) L(ine roughness) S(ensitivity) trade-off. However, after application of the DSA rectification process and etching into SiN for these three resist patterns, the uLWR value is reduced and remains constant throughout the tested dose range. In addition, the high defect density from resist#3 is completely healed after the DSA rectification process. As such, a reduction of the EUV working dose by over 60% can be observed without compromising roughness or defectivity.

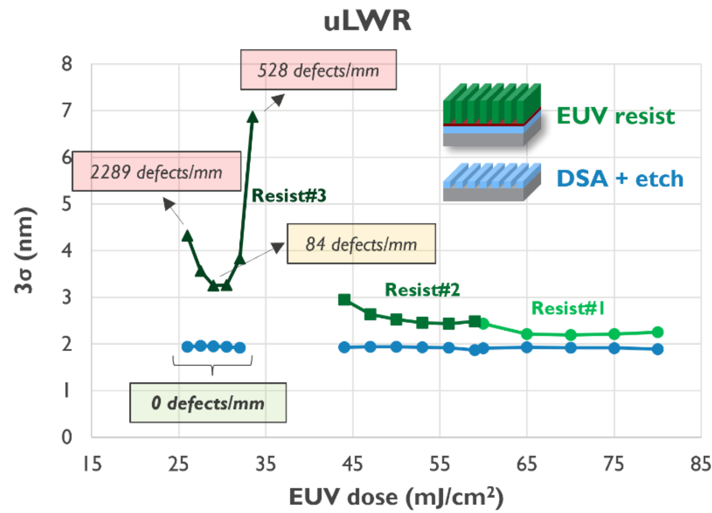

Figure 1. uLWR *vs.* EUV dose for a pitch 28 nm L/S pattern as measured from three different CAR resist patterns after EUV exposure and development (green) and after DSA rectification and etch into a SiN layer (blue). Compared to resist#1, EUV dose can be reduced by more than 60% without noticeable impact on roughness or defectivity. Defect values are extracted from 50 CDSEM images.

In our previous work, it was shown that bridge defects are the main defect type observed from DSA rectified patterns after pattern transfer into a SiN hard mask.[8,9] Therefore, a systematic study on the origin of bridge defect formation in the DSA patterns is desired. To this end, we first evaluate the impact of BCP material formulation. Figure 2 illustrates a strong correlation between the BCP material formulation and bridge defect density down to an inflection point below which bridge defect density decreases much less rapidly. Instead, below this inflection point, line pinching starts to occur indicating that these BCP formulations are no longer favorable. Therefore, it is hypothesized that the inflection point corresponds to the optimal BCP formulation. The residual bridge defects observed at point should be mitigated in different ways.

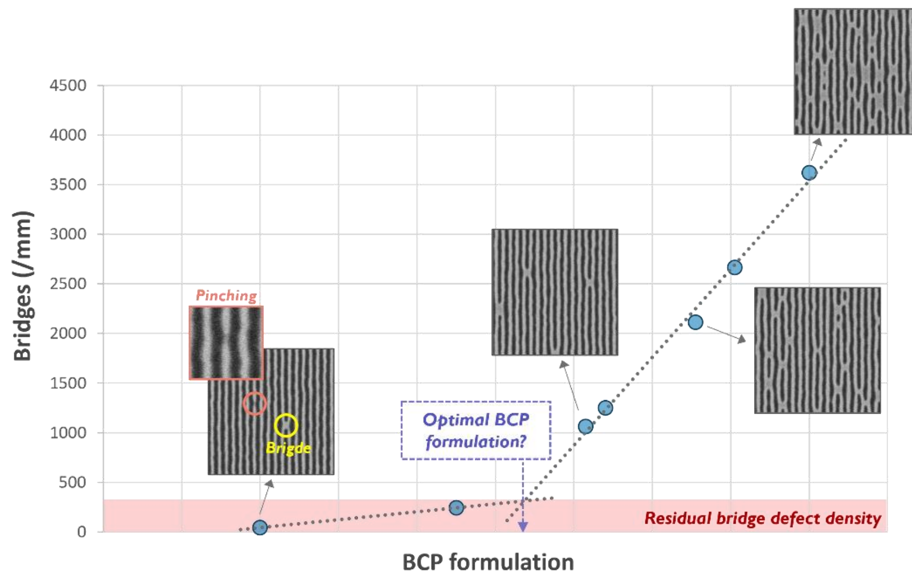

Figure 2. Relation between bridge defect density of a pitch 24 nm L/S DSA pattern and the BCP material formulation. Bridge defect density is measured from evaluation of 30 CDSEM images as described in the methods section. The inflection point is hypothesized to correspond to the optimal BCP formulation.

Besides the BCP material formulation, it can be considered that the choice of the DSA underlayer material, and thus indirectly the DSA guide pattern properties, has an important impact on the observed bridge defect density as well. To test this idea, five different underlayer materials were selected in addition to the baseline X-PS underlayer. The polar and dispersive components of the surface energy were measured for the pristine underlayers, as well as after application of the surface treatment to each underlayer as described in the methods section. The obtained values are shown in Figure 3a and the wetting behavior towards polystyrene (PS) or polymethylmethacrylate (PMMA), which is estimated from the parameter $\Delta\gamma$, is visualized by the red and blue color in the graph, respectively. The difference in wetting preference before and after the surface treatment, referred to as the contrast of $\Delta\gamma$, is directing the self-assembly process and is therefore believed to play a significant role in controlling the final pattern quality. The contrast of $\Delta\gamma$ is quantified in Figure 3b. From this graph, it is clear that the largest contrast of the guide pattern is obtained from the X-PS underlayer. This large guide pattern contrast for X-PS mainly originates from the larger response to the polar surface treatment compared to the other underlayer materials. Next, pitch 28 nm L/S DSA patterns were prepared on each underlayer, and defectivity was measured by optical inspection followed by e-beam review. From the obtained defect data shown in Figure 3c, it can be observed that the lowest bridge defect density and overall best defectivity is observed on the X-PS underlayer. Interestingly, there is a strong inverse relation with the contrast of the DSA guide pattern and final defect density. On underlayer E, no DSA could be achieved because of the weak guide pattern contrast. From this study, it can be concluded that (bridge) defects can be mitigated by maximizing the contrast of the guide pattern. This may provide room for further improvement by optimizing the underlayer as well as the polar surface treatment step.

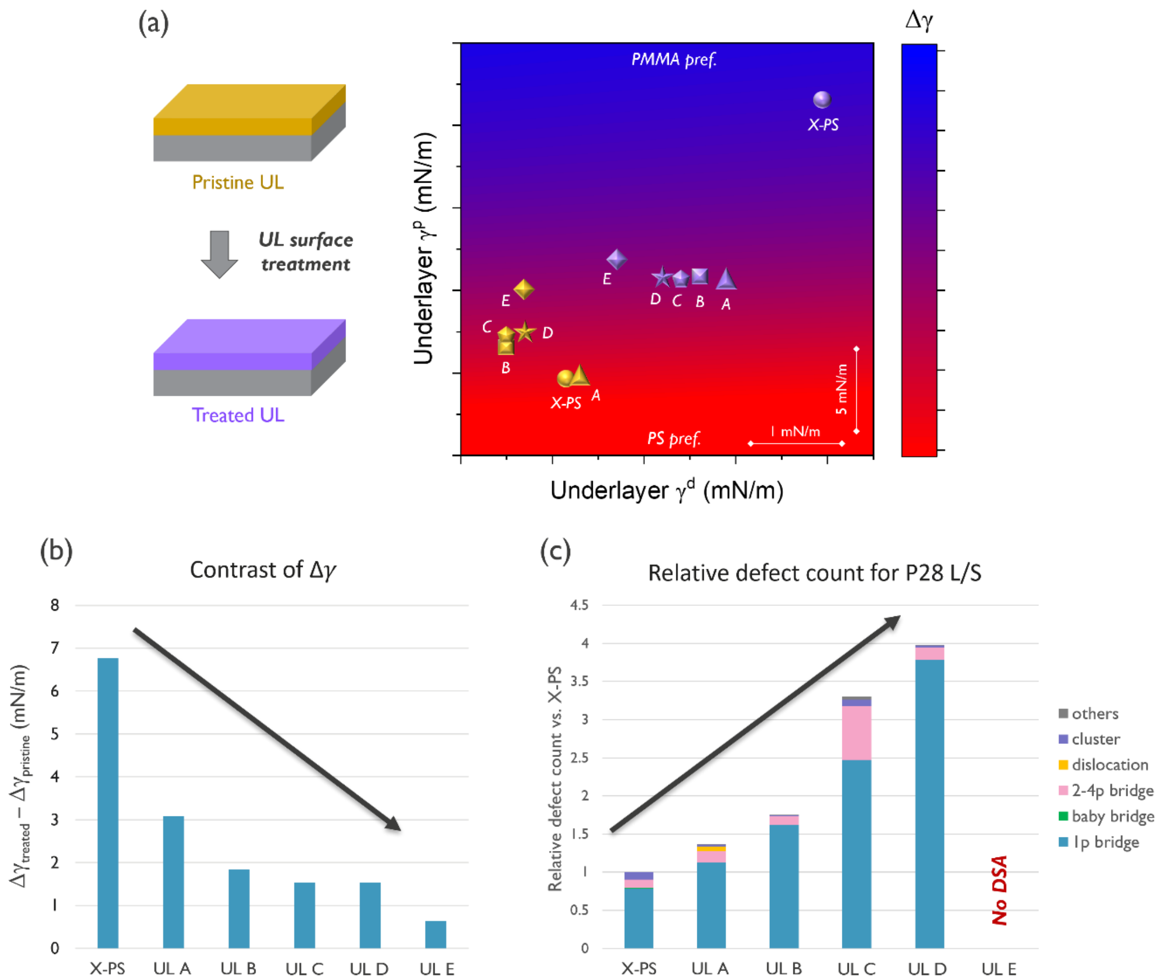

Figure 3. (a) Plot of the surface energy for each underlayer as measured without (pristine, yellow) and with (treated, purple) application of the polar surface treatment. $\Delta\gamma$ refers to the preferred wetting behavior of the underlayer, with preferential PS wetting colored in red and preferential PMMA wetting colored in blue. (b) The contrast of $\Delta\gamma$ indicating the guide pattern strength for each underlayer. (c) Relative defect count *vs.* X-PS for a pitch 28 nm L/S DSA pattern prepared on different underlayers. On underlayer E, no defect data are available as we could not observe DSA on this guide pattern. In general, a strong inverse correlation is observed between the strength of the guide pattern (contrast of $\Delta\gamma$) and the final defectivity of the pitch 28 nm L/S DSA pattern.

2.2 HEXCH pattern rectification

The pattern quality of HEXCH patterns can be quantified by the LCDU and LPPE value. As shown in previous work, the LCDU can be significantly improved by DSA rectification.[8] However, controlling the LPPE of DSA patterns was identified as one of the main challenges. To this end, six different BCP materials were compared for rectification of a pitch$_{C2C}$ 32 nm HEXCH EUV resist pattern. As shown in Figure 4a and 4b, both LCDU and LPPE can be reduced at the same time by optimization of the BCP material formulation. Benchmarking the best DSA pattern (after etching into SiN) as obtained by BCP F versus the original EUV resist pattern shows better LCDU but slightly worse LPPE as shown in Figure 4c. To get the overall picture, LCDU and LPPE can be combined in one metric referred to as the local edge placement error (LEPE). As shown in Figure 4c, DSA rectification with the optimized BCP material formulation results in an overall improvement of the LEPE. It needs to be noted though that we are comparing the DSA pattern after etching into SiN *versus* the EUV resist pattern after development. As such, the impact of DSA rectification is convoluted with the pattern transfer etch. A fairer comparison would be to evaluate the EUV resist patterns after etching into the same SiN layer.

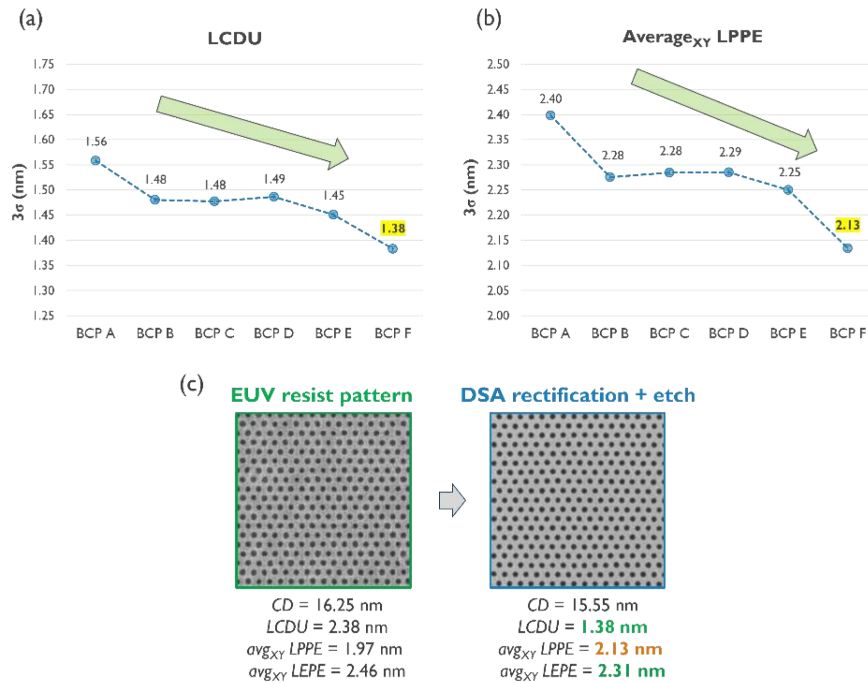

Figure 4. (a,b) LCDU and LPPE measured for pitch$_{C2C}$ 32 nm HEXCH patterns after DSA rectification and etching into SiN. Six different BCP material formulations were considered. All BCP materials were annealed at 260 °C for 30 min. (c) Benchmarking the EUV resist pattern *versus* the best DSA rectified pattern obtained with BCP F (after SiN etch). An overall improvement of LEPE can be observed after DSA and etch.

Next, the DSA alignment window as a function of resist CD and BCP anneal temperature was determined for BCP F. As shown in Figure 5b, the BCP can only be properly aligned on a pitch$_{C2C}$ 32 nm guide pattern for an anneal temperature ranging from 230 °C to 270 °C. At 210 °C, the BCP is still oriented mainly perpendicular to the surface but can no longer be aligned to the guide pattern. This lack of alignment can be explained by a mismatch between the target pitch and the increasingly large L_0 value of the BCP at lower temperature as shown in Figure 5a. On the other hand, at 290 °C, a parallel orientation of the BCP to the surface is observed, which indicates that the boundary conditions are no longer favorable for DSA at this high temperature.

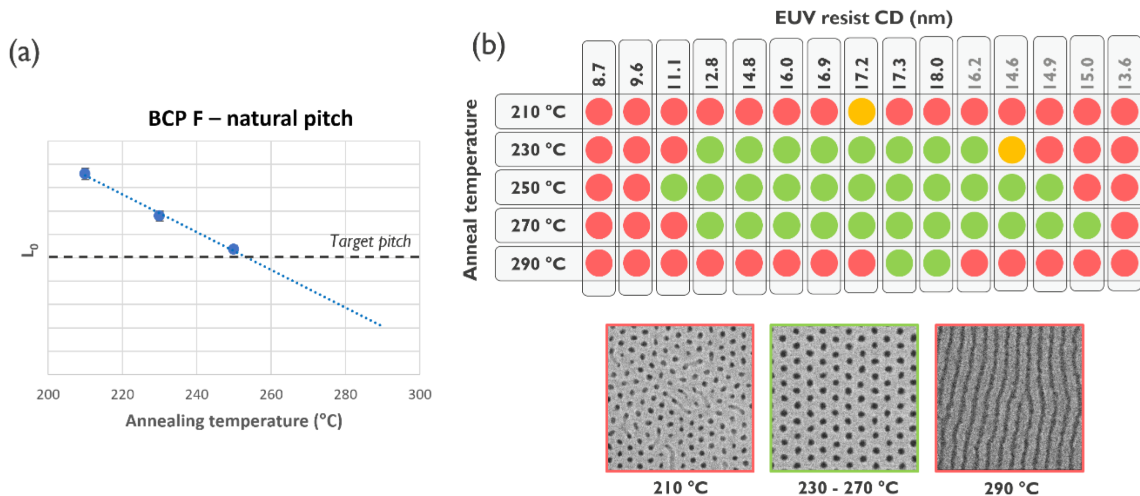

Figure 5. (a) L_0 of BCP F as a function of the anneal temperature. Target pitch$_{C2C}$ is 32 nm. The dotted line represents a linear fit to the measured data points. (b) Alignment window of BCP F as a function of EUV resist CD and BCP anneal temperature. The green color represents proper BCP alignment. The BCP anneal time was set to 3 min.

Given the alignment window for BCP F shown in Figure 5b, defectivity of the DSA patterns after etch was measured by e-beam inspection for three different BCP anneal temperatures. As shown in Figure 6a, the defect window is shifting towards larger resist CD values as the BCP anneal temperature increases. In Figure 6b, the defects are classified according to the defect type. Whereas at lower BCP anneal temperature, partially closed holes are predominantly observed, missing holes are more likely to occur at higher anneal temperature. At an intermediate temperature of 250 °C, both types are observed. Finally, we collected 7500 e-beam images for an anneal temperature of 250 °C and at the center of the defect window. From this large area inspection, zero defects were detected out of approximately 31 million inspected holes. Based on this result, it can be concluded that a defect level of less than 10^{-7} defective holes can be obtained by working in the center of the BCP alignment window.

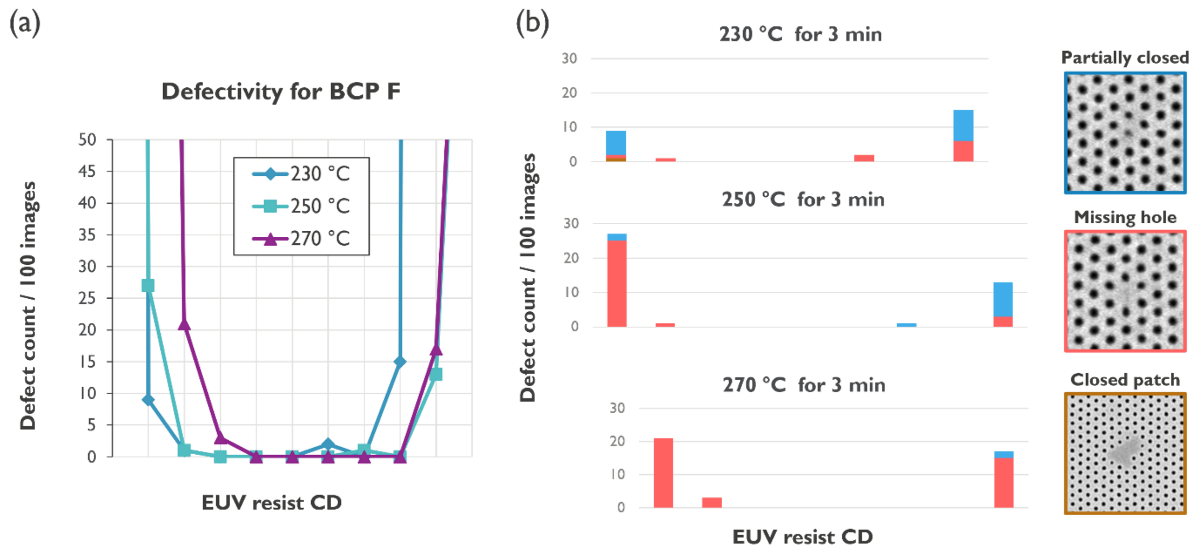

Figure 6. Defectivity for pitch$_{C2C}$ 32 nm DSA patterns with BCP F after etching into SiN. Anneal time is set to 3 min. (a) Defect count from 100 e-beam images as a function of resist CD. (b) Classification of defect types as function of resist CD and BCP anneal temperature. E-beam images were obtained with a 2 μm×2 μm field of view.

Finally, the DSA rectification process for HEXCH patterns was scaled down to pitch$_{C2C}$ 30 nm. This pitch is close to the physical limit for printing a HEXCH pattern on the 0.33NA EUV tool. To perform rectification of the EUV resist pattern, four different BCP materials were tested. Figure 7a depicts the L_0 values as a function of the applied anneal temperature for each BCP. As evident from the graph, three different L_0 values are available, with BCP A having the smallest size and BCP C being the largest. BCP B has intermediate size. For the latter, a second formulation is also available referred to as BCP B'. The patterning performance of each BCP material was subsequently evaluated by extracting the LCDU and LPPE after rectification as shown in Figure 7b,c. It can be observed that BCP B' exhibits larger LCDU and LPPE than the other materials indicating that this alternative material formulation is not favorable. In addition, it appears that the better LPPE is obtained from the BCP with the largest natural pitch.

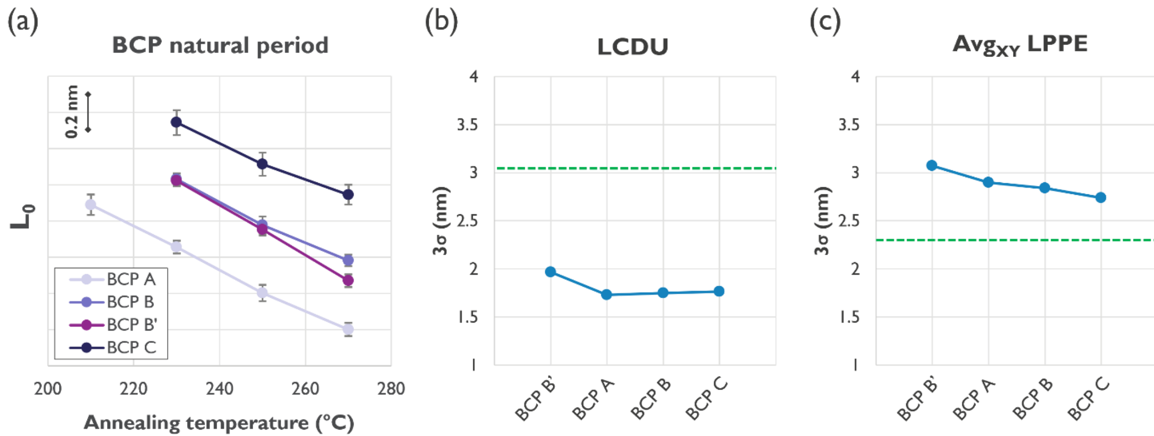

Figure 7. Rectification of pitch$_{C2C}$ 30 nm HEXCH patterns. (a) Measurement of L_0 as a function of BCP anneal temperature for four different BCP materials. All BCP materials were baked at 250 °C for 5 min. (b,c) LCDU and LPPE of the DSA rectified patterns after etching into a SiN layer. The green dotted line represents the value measured from the EUV resist pattern for reference.

Finally, the rectification performance at pitch$_{C2C}$ 30 nm was evaluated as function of different annealing temperatures using BCP A, B, and C. The results for LCDU and LPPE are shown in Figure 8. Within the tested temperature range, it can be observed that better LCDU and LPPE are obtained at lower BCP anneal temperature. Given that in previous paragraph better LPPE was obtained with the BCP having the largest L_0 value, the results shown here can be attributed to the fact that at lower anneal temperature, the natural pitch of the BCP is becoming larger.

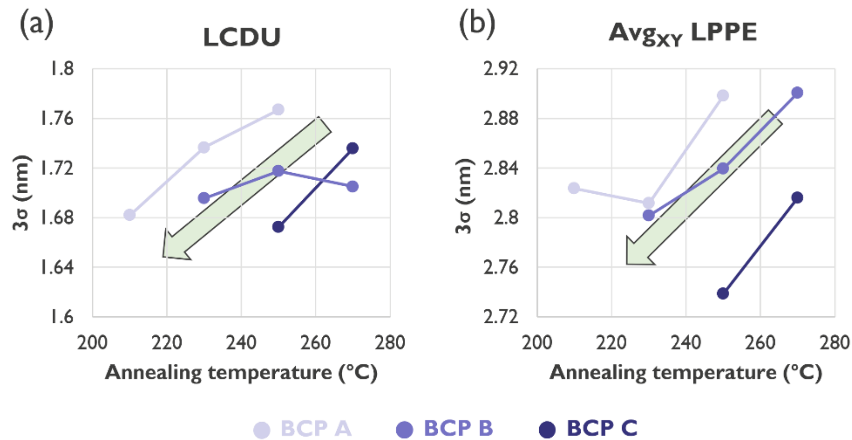

Figure 8. Rectification of pitch$_{C2C}$ 30 nm HEXCH patterns as function of the anneal temperature for three different BCP materials. The annealing time was set to 5 min. (a,b) LCDU and LPPE measured after rectification and etching into SiN. The green arrows indicate that lower LCDU and LPPE are generally obtained at lower BCP anneal temperature.

4. CONCLUSIONS

In conclusion, we have presented several material and process contributions towards optimizing the DSA rectification process for L/S and HEXCH patterns. A reduction of EUV dose by 60% without compromising roughness or defectivity for a pitch 28 nm L/S pattern was demonstrated. Furthermore, the impact of BCP and underlayer material on bridge defect density were discussed. Based on our study, it is concluded that the best defectivity can be obtained by optimizing the BCP

material formulation and maximizing the contrast of the DSA guide pattern. Next, it was shown how LCDU and LPPE for a $pitch_{C2C}$ 32 nm HEXCH pattern can be improved simultaneously by optimization of the BCP material. For the best performing BCP, a detailed defect inspection was conducted showcasing that a defect density below 10^{-7} defective holes can be obtained by operating in the center of the BCP alignment window. Finally, rectification of $pitch_{C2C}$ 30 nm HEXCH patterns was demonstrated, with overall best performance for larger BCP L_0. The next step includes optimization of the etch and stack, especially to further improve roughness and defectivity of L/S patterns.

ACKNOWLEDGEMENTS

The authors are grateful to the material suppliers for providing DSA materials in the framework of joint development projects. The authors also kindly acknowledge the support for BCP processing by the track tool supplier. Hitachi High Tech is kindly acknowledged for providing the DSA-APPS software package. The technical support of imec colleagues Nadia Vandenbroeck and Jelle Vandereyken is also kindly acknowledged.

REFERENCES

[1] Ito, H., “Rise of chemical amplification resists from laboratory curiosity to paradigm enabling Moore’s Law,” Proc. SPIE 6923, 692302 (2008).

[2] De Silva, A., Meli, L., Goldfarb, D. L. and Felix, M., "Fundamentals of resist stochastics effect for single-exposure EUV patterning,” Proc. SPIE 10957, 109570F (2019).

[3] Fallica, R., Haitjema, J., Wu, L., Castellanos, S., Brouwer, A. M. and Ekinci, Y., “Absorption coefficient of metal-containing photoresists in the extreme ultraviolet,” J. Mirco/Nanolith. MEMS MOEMS 17, 023505 (2018).

[4] Fallica, R. and Ekinci, Y., “Photoacid generator-polymer interaction on the quantum yield of chemically amplified resists for extreme ultraviolet lithography,” J. Mater. Chem. C. 6, 7276 (2018).

[5] Stoykovich, M. P., Daoulas, K. C. Muller, M., Kang, H., de Pablo, J. J., Nealey, P. F., "Remediation of line edge roughness in chemical nanopatterns by the directed self-assembly of overlying block copolymer films," Macromolecules 43, 2334-2342 (2010).

[6] Ruiz, R., Kang, H., Detcheverry, F. A., Dobisz, E., Kercher, D.S., Albrecht, T. R., de Pablo, J. J. and Nealey, P. F., “Density multiplication and improved lithography by directed block copolymer assembly," Science 321 (5891), 936-939 (2008).

[7] Suzuki, M., Kim, Y., Her, Y., Wu, H., Si, K., Maturi, M. M., Fackler, P. H., Moinpour, M., Dammel, R., Cao, Y., “Negative-tone resists for EUV lithography,” Proc. SPIE 12498, 1249813 (2023).

[8] Verstraete, L. Suh, H. S., Van Bel, J., Timi, P. H., Vallat, R., Bezard, P., Vandereyken, J., Beggiato, M., Tamaddon, A. H., Beral, C., Li, W., Gupta, M. and Fallica, R., “Mitigating stochastics in EUV lithography by directed self-assembly,” Proc. SPIE 12497, 12497OI (2023).

[9] Van Bel, J., Verstraete, L., Suh, H. S., De Gendt, S., Bezard, P., Vandereyken, J., Li, W., Beggiato, M., Tamaddon, A. H., Beral, C., Santos, A., Alperson, B. and Her, Y., "EUV lithography line-space pattern rectification using block copolymer directed self-assembly: a roughness and defectivity study," Proc. SPIE 12497, 12497OK (2023).

[10] Suh, H. S., Kang, H. Nealey, P. F. and Char, K., “Thickness dependence of neutral parameter windows for perpendicularly oriented block copolymer thin films,” Macromolecules 43, 4744-4751 (2010).

[11] Dehaerne, E., Dey, B., Esfandiar, H., Verstraete, L., Suh, H. S., Halder, S., De Gendt, S., “YOLOv8 for defect inspection of hexagonal directed self-assembly patterns: a data-centric approach,” Proc. SPIE 12802, 128020S (2023).